Three-Dimensional Visualization and Presentation of Bridge Deck Condition Based on Multiple NDE Data

Jinyoung Kim, Ph.D.[1]; Nenad Gucunski, Ph.D., A.M.ASCE[2]; Trung H. Duong, Ph.D.[3]; and Kien Dinh, Ph.D., A.M.ASCE[4]

Abstract: A method is developed for presentation of a concrete bridge deck condition assessed by multiple nondestructive evaluation (NDE) technologies using a three-dimensional (3D) visualization program. Four types of NDE data are merged and visualized in the program: (1) impact echo for mapping and describing the severity level of concrete delamination; (2) ultrasonic surface wave for concrete quality (elastic modulus) assessment; (3) electrical resistivity for estimating the corrosion rate of steel reinforcement; and (4) high-resolution imaging of a bridge deck surface for documenting signs of deterioration, previous repairs, and surface wear. The developed visualization platform integrates the four NDE data types and visualizes in a 3D space in a very intuitive way. As such, the program assists in understanding of the complex relationships of bridge deck conditions assessed by multiple NDE techniques. In addition, a correlation between external (surface cracks, wear, and previous repairs) and internal deterioration (delamination, concrete degradation, and corrosion) can be studied and visually identified utilizing the developed 3D visualization program. **DOI: 10.1061/(ASCE)IS.1943-555X.0000341.**

Author keywords: Nondestructive tests; Bridge inspection; Bridge decks; Data analysis; Visual techniques; Concrete.

Introduction

Civil infrastructure systems such as roads, bridges, dams, power plants, and so on, provide vital functions for sustaining our society and are directly related to the economic growth and sustainability. Infrastructures, like a human body, age and deteriorate over time, not only due to a routine usage of the facilities, but also because of the environmental changes and exposure to extreme conditions. Therefore, infrastructure management requires periodic inspections and maintenance to achieve or retain required performance throughout the service life of an infrastructure asset. Because of the nature of civil infrastructure systems, which are massive in size and complexity, significant financial and other resources are required to maintain the existing civil infrastructures in good condition. According to a report by the U.S. Department of Transportation (USDOT 2014), 77,375 or 12.8% of the total number of bridges in the United States are functionally obsolete and 69,517 or 11.5% are structurally deficient. Bridges are, on average, over 40 years old, and $76 billion in total is required for their repair and replacement (ASCE 2013).

Due to the insufficient funding levels, it is inevitable that transportation agencies prioritize and selectively invest into infrastructure assets that need immediate attention. Therefore, it is essential to accurately and objectively assess the condition and identify the main deterioration causes by using accurate, rapid, and nondestructive condition assessment technologies. This will enable realistic prediction of the service life of infrastructures. There are a number of possible causes of rapid deterioration of civil infrastructures according to the recent reports (DHS 2010; ASCE 2013; USDOT 2014), including but not limited to overloading, freeze-thaw cycles, and corrosion of steel, among others. In the case of bridges, generally between 50 and 80% of the entire expenditures for maintenance and rehabilitation of bridge components are spent on bridge decks (Gucunski et al. 2013). Rebar corrosion is identified as the primary cause of deterioration of bridge decks (Russell et al. 2004).

Complexity attributed to the composite material nature of concrete and the variety of deterioration processes makes a comprehensive assessment of concrete bridge decks by a single NDE method pretty much impossible. Therefore, it is often required to use multiple NDE methods to assess the bridge deck condition. For example, electrical resistivity (ER) and half-cell potential (HCP) to estimate corrosion rate and activity of reinforcement, respectively, impact echo (IE) or ultrasonic pulse echo (UPE) to assess delamination, and ultrasonic surface wave (USW) to evaluate concrete quality. Currently, two-dimensional (2D) contour maps of individual NDE methods are often used to present the condition of the surveyed area. Therefore, the spatial correlation between the results from different NDE methods is hard to establish. To present the condition of bridge decks more effectively and to better correlate multiple NDE results, some of the recent works utilized three-dimensional (3D) visualization methods. Some examples include IE (Gucunski et al. 2008, 2012; Wiggenhauser 2009), ultrasonic (Schickert and Tümmler 2009), and combined techniques (Kohl et al. 2005). It is obvious that the combined NDE methods with data integration and fusion techniques in 3D provide enhanced means of data visualization by providing complementary results with synergistic effects between

[1]Assistant Professor, Dept. of Architectural Engineering, Ajou Univ., 206 Worldcup-ro, Yeongtong-gu, Suwon-si, Gyeonggi-do 16499, Republic of Korea. ORCID: http://orcid.org/0000-0001-5879-8607. E-mail: jinyoungkim@ajou.ac.kr

[2]Professor and Chair, Dept. of Civil and Environmental Engineering, Rutgers, 96 Frelinghuysen Rd., Piscataway, NJ 08854 (corresponding author). E-mail: gucunski@rci.rutgers.edu

[3]Research Associate, Center for Advanced Infrastructure and Transportation, Rutgers, 100 Brett Rd., Piscataway, NJ 08854. E-mail: duonghuytrung@gmail.com

[4]Research Associate, Center for Advanced Infrastructure and Transportation, Rutgers, 100 Brett Rd., Piscataway, NJ 08854. E-mail: dinhkien_huce@yahoo.com

Note. This manuscript was submitted on September 4, 2015; approved on August 2, 2016; published online on October 31, 2016. Discussion period open until March 31, 2017; separate discussions must be submitted for individual papers. This paper is part of the ***Journal of Infrastructure Systems***, © ASCE, ISSN 1076-0342.

individual survey results. As such, they are enabling detection of deteriorated areas in a 3D space with higher confidence levels.

In this study, a method is developed for presentation of a concrete bridge deck condition using a 3D visualization program, *NDEFuse*. The program integrates four types of NDE data: (1) IE data for mapping and describing the severity level of concrete delamination; (2) USW data for concrete quality (elastic modulus) assessment; (3) ER data for the description of the corrosive environment and estimation of the corrosion rate of reinforcement; and (4) high-resolution imaging of bridge deck surface for documenting signs of deterioration, previous repairs, and surface wear. The integrated NDE data are visualized in a 3D space in a very intuitive manner to facilitate comprehensive presentation and understanding of the overall condition of a bridge deck.

Bridge Deck Inspection and Data Presentation

A brief description of operation and typical data presentation for each of the four NDE technologies (IE, USW, ER, and surface imaging) are provided in the following sections. The data-processing methods to expand the NDE data presentation from 2D condition maps to 3D volumes are described using the actual survey results for a bridge deck. The selected deck is the one of Madison Highway (Virginia Rt. 15) over I-66 Bridge (National Bridge Inventory Structure Number 000000000014178) in Haymarket, Virginia. Validation of the condition assessment using the coring samples was not done at the time of the survey. However, the performance of NDE technologies was validated on the same bridge during the SHRP 2 R06-A project (Gucunski et al. 2013), and the research team has previously validated their performance on a number of bridges (Gucunski et al. 2011, 2012, 2015b). In addition, prior to the survey of the bridge deck, performance of all NDE technologies was evaluated on the validation slab on one of the Rutgers campuses (Gucunski et al. 2015b). A validation bridge structure was built with various types of artificial defects, and the NDE test and data-processing methods adopted in this study were successfully validated (Gucunski et al. 2012, 2013, 2015b). The bridge deck was surveyed in October of 2014. The bridge was constructed in 1979 as a two-span continuous steel girder with a bare concrete deck of approximately 22 cm thick. The NDE data collection was conducted by point testing on a 60×60 cm test grid with the first longitudinal line of the grid offset 30 cm from the parapet.

Delamination Assessment Using Impact Echo

The IE test is primarily used to detect and assess the severity of delamination by identifying the reflectors of acoustic waves (Sansalone and Carino 1986). The IE test was conducted using an impact source (custom built linear-solenoid) and a nearby receiver

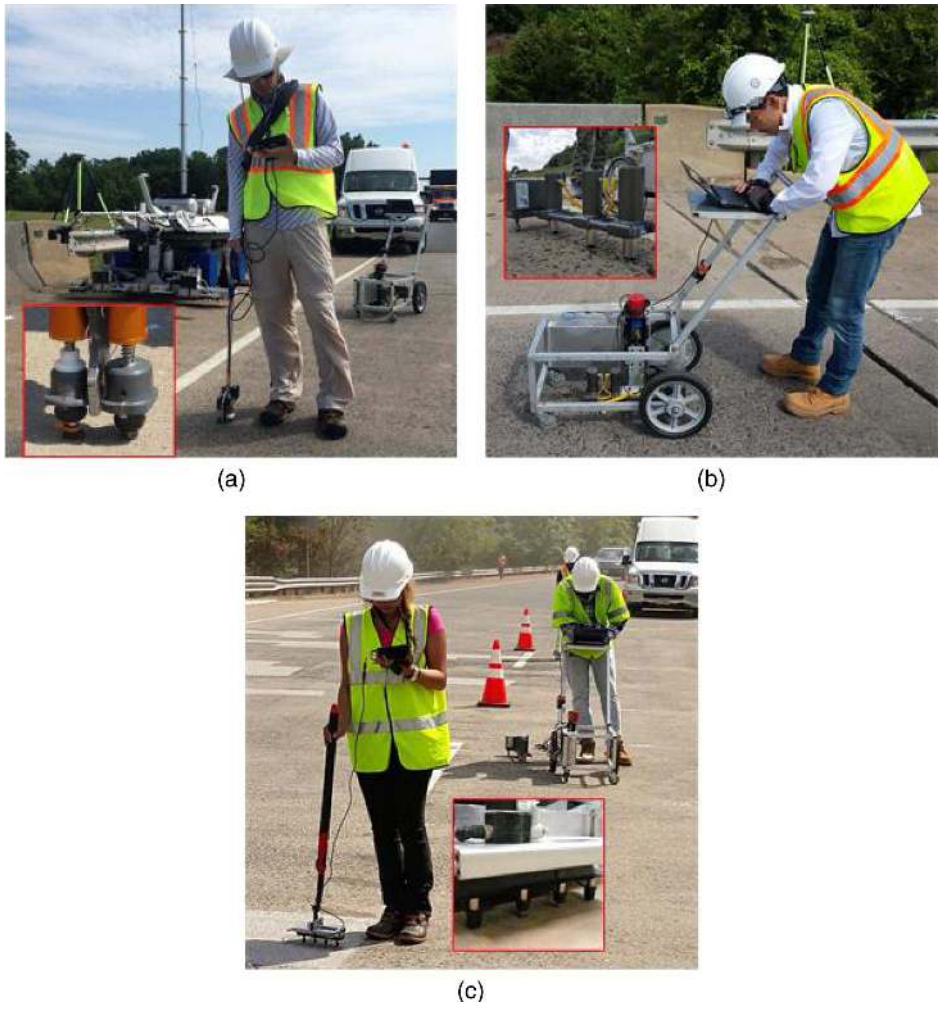

Fig. 1. NDE technologies (images by Jinyoung Kim): (a) impact echo testing; (b) ultrasonic surface wave testing using PSPA; (c) electrical resistivity testing using Resipod probe

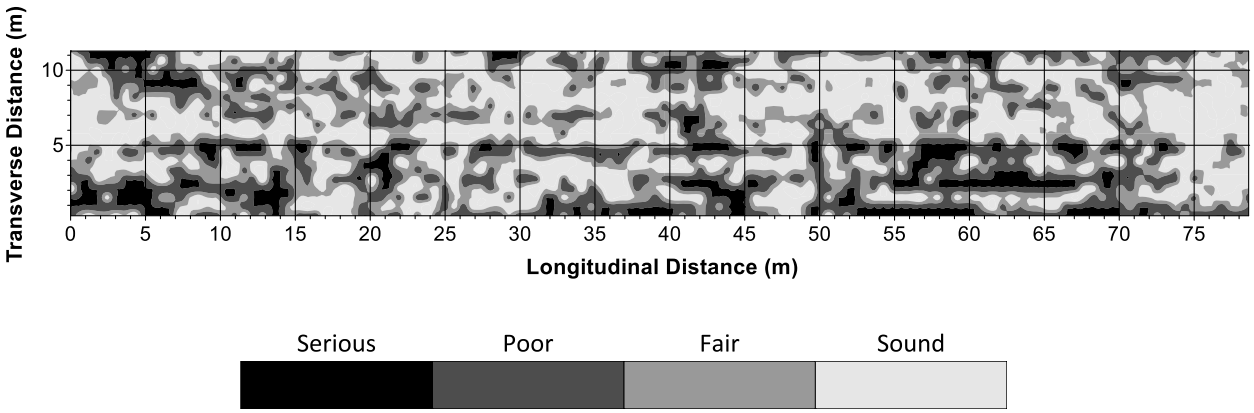

Fig. 2. Impact echo 2D delamination condition map

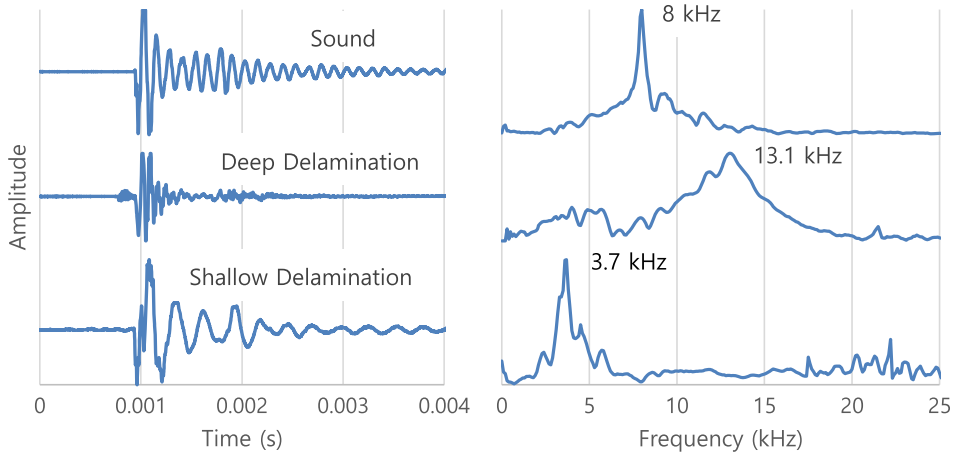

Fig. 3. Representative time responses and corresponding frequency spectra of sound area, deep delamination, and shallow delamination

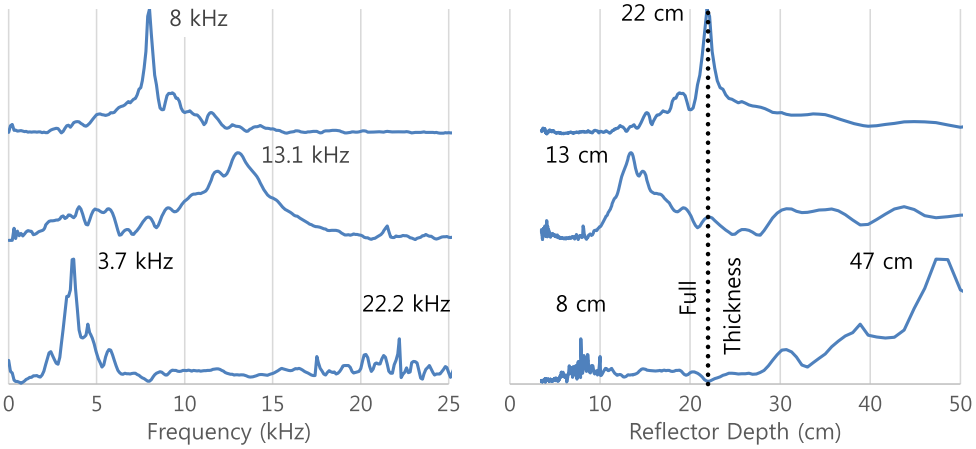

Fig. 4. Representative frequency spectra and corresponding depth spectra of deck bottom (top line), deep delamination (middle line), and shallow delamination (bottom line)

(PCB Piezotronics, Depew, New York, model 352C67, accelerometer). The receiver was connected to a battery-powered signal conditioner, which was connected to a data-acquisition unit through an USB interface. The spacing between the source and receiver was 7.5 cm [Fig. 1(a)]. The waves generated by the impactor are reflected at the bottom of the deck or at the delamination due to a large contrast in the acoustic impedance of concrete and air. The transient time response of the reflected waves is captured by the receiver, and converted into a frequency spectrum to identify the severity of delamination.

A conventional condition map of a deck with respect to delamination is shown in Fig. 2 for the deck of Madison Highway over

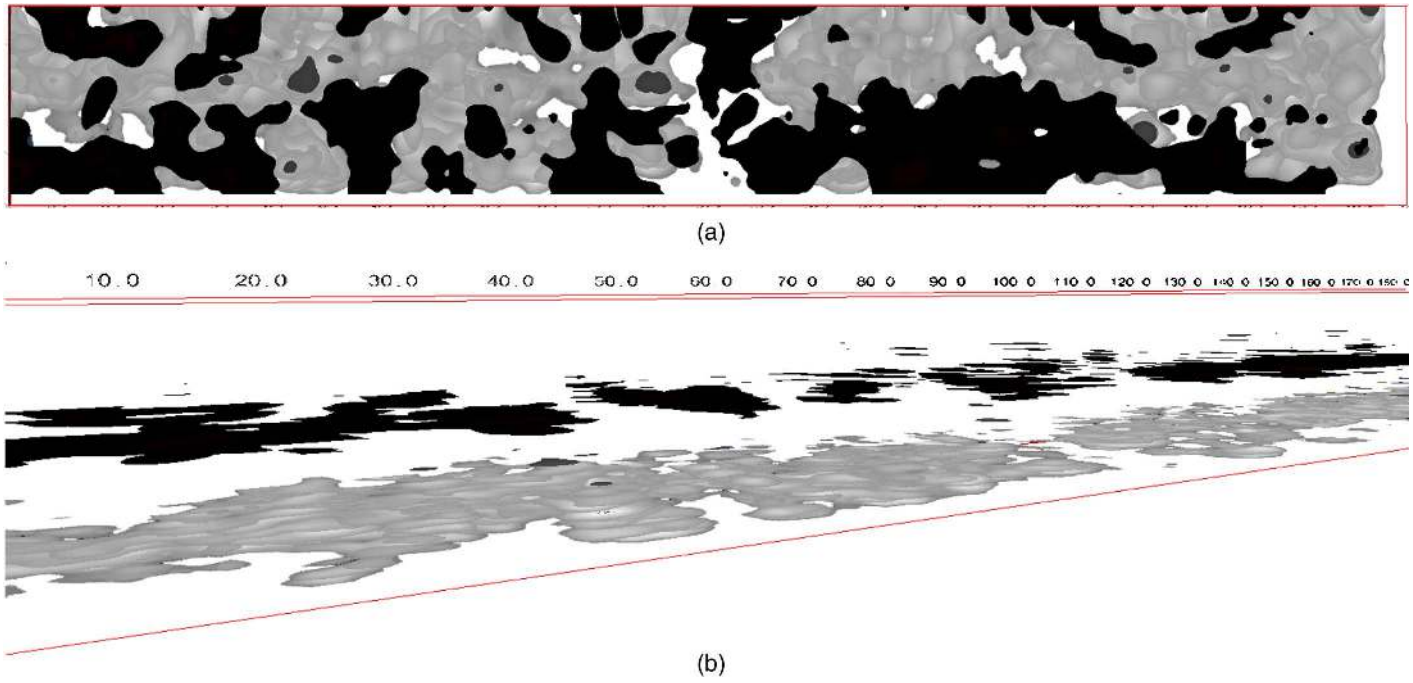

Fig. 5. Impact echo 3D condition map displaying delamination severity and depth through *NDEFuse* (shallow delamination, deep delamination, and the bottom of the deck are visualized in black, dark gray, and light gray, respectively): (a) top view of the entire bridge deck; (b) a portion of the deck in 3D view

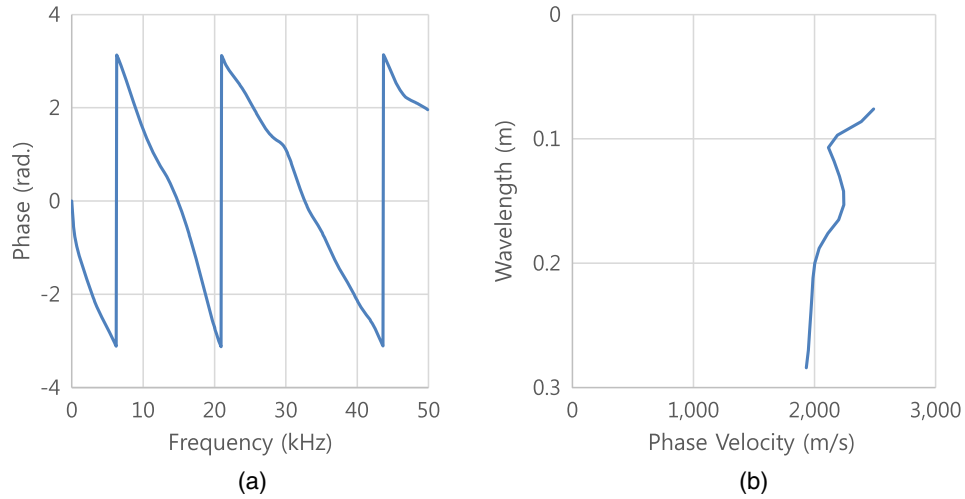

Fig. 6. Relation between (a) wrapped phase and frequency and (b) obtained dispersion curve

I-66 Bridge. The condition map was created based on the 2D IE data grid (60 × 60 cm) using a commercial surface mapping software, *Surfer*, by Golden Software, with a color scale of four levels: sound, fair, poor, and serious. The four levels were graded from 1 (sound) to 4 (serious). The serious (shallow or wide delamination) and poor (small or deep delamination) conditions are indicated in the figure as black and dark gray, respectively. The areas in fair and sound conditions are presented in medium and light gray, respectively. Representative signal responses in the time domain, and the corresponding frequency spectra, measured over a solid region, deep and shallow delamination are shown in Fig. 3. When an IE test is conducted over a sound area, a clear peak in the frequency response around 8 kHz is obtained. Deep delamination makes the peak shift toward a higher frequency range, whereas much lower frequency is obtained for shallow (fully developed) delamination due to the flexural oscillation mode of the thin concrete section above the delamination. Depending on the delamination extent, continuity, and size, the partitioning of the wave energy reflected from the delamination may vary, causing the peak frequency shift. In this study, for a practical purpose, the in-depth consideration of the effects of frequency shift as a result of wave scattering around the edges of a small delamination, relative to the depth, was not included.

The IE data can also be used to identify the position of the wave reflectors (Sansalone and Carino 1986; Gucunski et al. 2008, 2012). The depth of wave reflectors can be calculated from

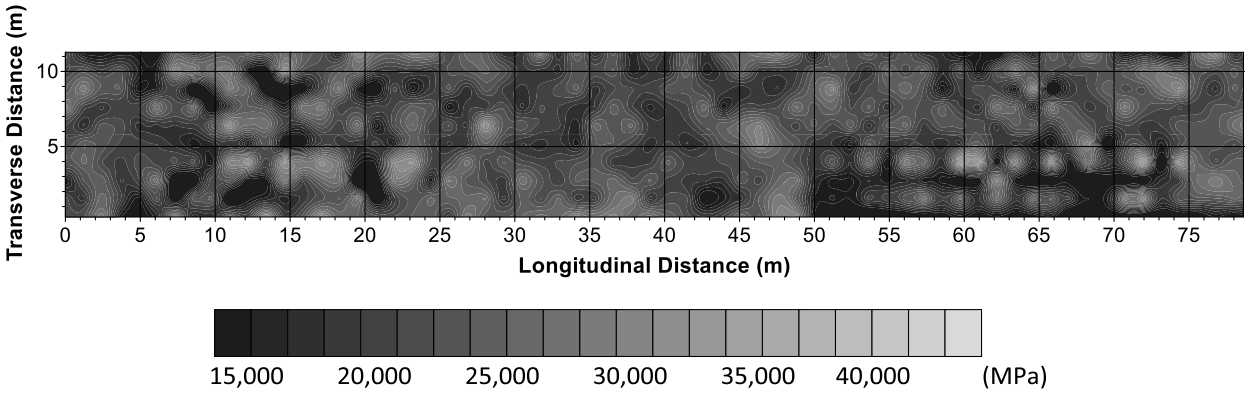

Fig. 7. 2D map of the concrete elastic modulus by ultrasonic surface wave test

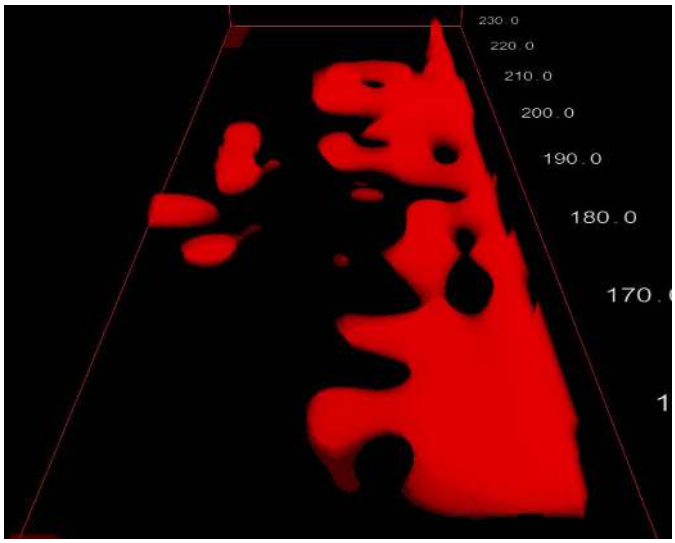

Fig. 8. 3D map of the concrete elastic modulus emphasizing the area with modulus less than 20 GPa utilizing *NDEFuse*

Table 1. Relationship between Electrical Resistivity and Corrosion Rate (Data from Langford and Broomfield 1987)

Electrical resistivity (kΩ · cm)	Corrosion rate
<5	Very high
5–10	High
10–20	Moderate–low
>20	Low

$$\text{Depth of wave reflector} = \beta \frac{C_P}{2f_{\text{peak}}} \tag{1}$$

where β = correction factor ranging 0.945–0.957 for normal concrete (Gibson and Popovics 2005); C_p = compression (primary or P-) wave velocity of concrete; and f_{peak} = peak frequency. Using the equation, the relation between frequency and depth can be established for every component of a frequency spectrum with an assumed value of C_p. Representative frequency spectra and converted thickness spectra are shown in Fig. 4 for the full depth of 22 cm, deep delamination with the depth of the reflector shallower than the full thickness, and a shallow delamination. For a shallow delamination, as described earlier in Fig. 3, the peak amplitude is observed at a low frequency (3.7 kHz) due to the flexural oscillations. This makes the converted depth to be even deeper than the full depth of the deck. Therefore, a simple conversion of a peak frequency into depth of wave reflector using Eq. (1) would not provide the correct depth for a shallow delamination. To overcome the incorrect thickness conversion and to properly visualize those areas where low frequencies are dominant, efforts were made to obtain the actual depth of shallow delamination by detecting a secondary peak in a high frequency range (Gucunski et al. 2008, 2012). The secondary peak search was conducted within a depth range between 6 and 12 cm (corresponding frequency range of 17–33 kHz) for this bridge deck, and the amplitude and energy level of the second peak were also considered in the conversion algorithm. In the sample spectrum of a shallow delamination, the secondary peak was detected at 22 kHz, which was converted to 8 cm for an assumed value of $C_p = 4$ km/s, as shown in Fig. 4.

By converting the frequency into depth, the 2D IE condition map in Fig. 2 can be extended into a 3D space, where severity, location, and depth of delamination can be visualized together as shown in Fig. 5. In the figure, shallow delamination, deep delamination, and the bottom of the deck are visualized in black, dark gray, and light gray, respectively. The z-axis (depth) has been exaggerated to enable more effective visualization of both delamination and the deck bottom in the 3D view.

Concrete Quality Evaluation by Ultrasonic Surface Wave

The USW is used to measure the surface (Rayleigh or R-) wave velocity of concrete and ultimately to assess the quality of concrete in terms of elastic modulus. The USW test was conducted using the Portable Seismic Property Analyzer (PSPA) manufactured by Geomedia Research and Development, El Paso, Texas as shown in Fig. 1(b). The PSPA has a custom-made linear solenoid-type impact source and two piezoelectric accelerometers as receivers. The spacing between the impact source and near and far receivers was 10.2 and 25.4 cm, respectively. R-waves generated by an impact propagate along the deck surface with the velocity dependent on the elastic properties of concrete. The velocity of surface waves, termed phase velocity, is obtained from the phase of the cross-power spectrum (Fig. 6) for the receiver pair. Waves of different frequencies (wavelengths) travel with different velocities, illustrated by the dispersion curve in Fig. 6. This relationship can then be used to obtain the concrete modulus profile through an inversion process.

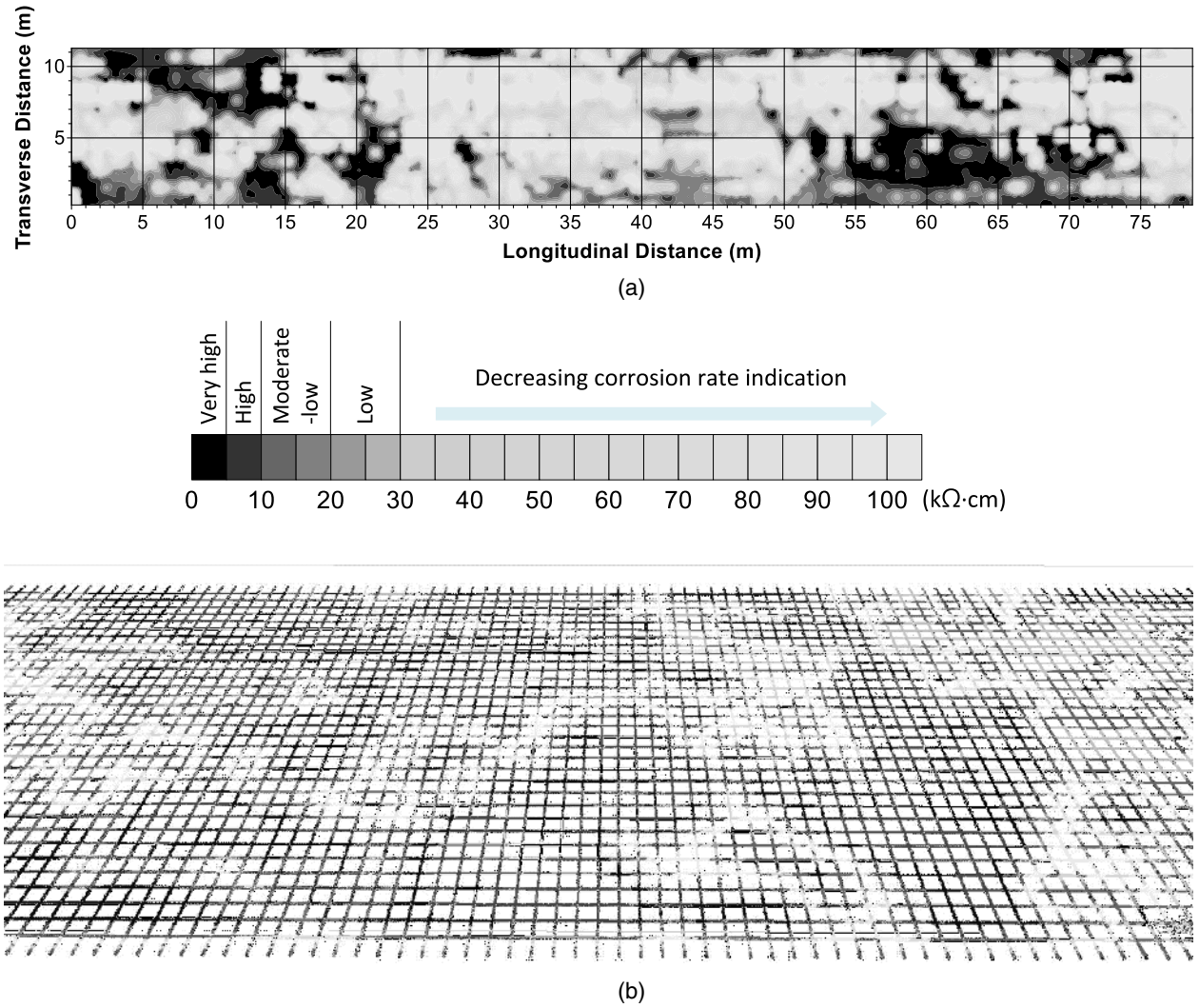

Fig. 9. Condition maps of electrical resistivity and expected corrosion rates: (a) 2D map of electrical resistivity and corrosion rates; (b) corrosion rates are displayed through shading of the top rebar layer in 3D electrical resistivity map in *NDEFuse*

Similar to the delamination condition map shown in Fig. 2, the concrete quality of the bridge deck in a 2D map was created based on the average concrete elastic modulus, and is shown in Fig. 7. Dark shades (black and dark gray) are indicators of a low concrete elastic modulus, and the shades shift toward lighter intensities (medium and light gray) as the modulus increases. Fig. 8 shows a closer view of the 3D volume of concrete with low elastic modulus. The shown section of the bridge deck extends from 50 m to the end joint in the longitudinal direction. In this 3D visualization, only the concrete volumes with the modulus lower than 20 GPa are displayed. Unlike the 2D presentation of elastic modulus using the average value for the deck thickness (Fig. 7), the 3D presentation involves modulus distribution with the depth matching the dispersion curves. Such a presentation provides only an approximate variation of modulus with depth. The correct information about the variation of modulus with depth can be obtained only through the process of back calculation.

Corrosion Assessment Using Electrical Resistivity

The ER is defined as how strongly a material opposes the flow of electric current (Whiting and Nagi 2003). In the evaluation of a concrete bridge deck, the ER test is used to assess the severity of concrete's corrosive environment and to estimate the corrosion rate of embedded reinforcing steel. The ER test was conducted utilizing the Resipod resistivity meter manufactured by Proceq, Zurich, Switzerland [Fig. 1(c)]. It is a fully integrated Wenner type probe (Wenner et al. 1915) with four equally spaced (5 cm) electrodes. Concrete is generally classified as an insulator when completely dry and semiconductor when saturated, exhibiting a wide range of resistivity depending on the moisture content, and the conductivity of the saturating fluid (Whiting and Nagi 2003). Generally, a hardened concrete saturated in salt water exhibits ER in the range of 0.25–100 $k\Omega \cdot cm$ (Lu 1997; Kim 2013). For the application of a concrete bridge deck evaluation, it has been reported that areas with ER lower than 5 $k\Omega \cdot cm$ are expected to have very rapid corrosion of rebar, while areas with ER over 100 $k\Omega \cdot cm$ would have negligible amounts of corrosion activity (Langford and Broomfield 1987; Dyer 2014). A commonly used relationship between the ER and corrosion rate is given in Table 1. It should be stressed that ER measurements using the Wenner probe for the assessment of severity of corrosive environment within concrete are very much dependent on its composite material nature. Because the measurement is of a volume of concrete close to the surface, ER can be affected by a number of factors that are not representative of the bulk concrete (Gowers and Millard 1999; Dyer 2014). Factors

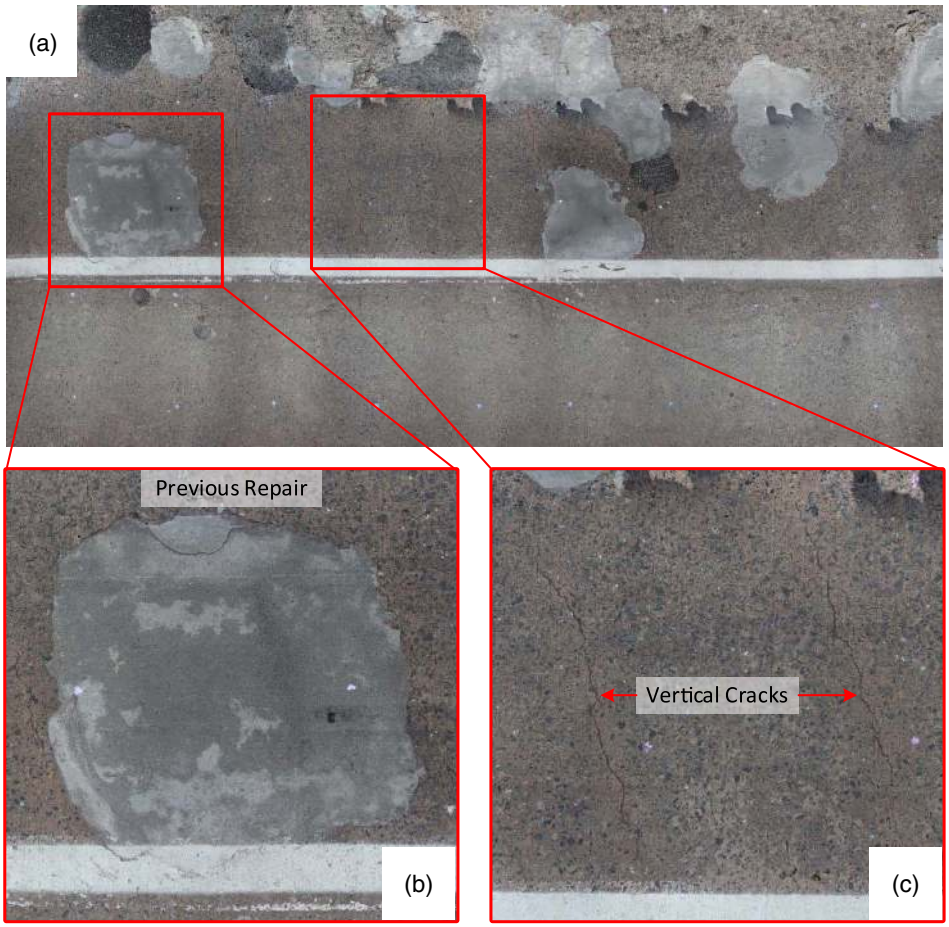

Fig. 10. Surface images of the bridge deck: (a) stitched image of 6×3 m^2 section of the bridge deck surface; (b) a closer view of 1.2×1.2 m^2 sections showing previous repair; (c) surface cracks

include moisture level, temperature, chloride content, location of rebar, and more. Especially due to the fact that moisture or chloride content in concrete is unknown at the time of the survey, the ER measurements with a given test setup may only be used to describe the cumulative effect on the concrete's electrical resistivity. Application and correlation of ER data with technologies that evaluate the rebar corrosion rate, like galvanostatic pulse measurement (GPM), would enable more reliable correlation of ER values and corrosion rates.

Fig. 9(a) shows the conventional 2D condition map of ER with expected corrosion rates based on the relationship listed in Table 1, created using *Surfer*, and Fig. 9(b) shows a closer view of the ER map in the *NDEFuse* 3D interface. In the ER condition maps, the shades change from black to light gray as the corrosion rate decreases or ER increases. In the 3D ER map, the corrosion rates are displayed through shading of the top rebar layer. In addition to visualizing in a 3D space, presenting the ER condition by the mapping of the rebar provides a number of advantages. The top rebar layout can be visually identified in a 3D space; for example, concrete cover depth (location of the top rebar layer), rebar spacing, and diameter of rebar as can be depicted in Fig. 9(b). The information about the actual layout and size is obtained from either design documents or ground penetrating radar surveys. If none of the data is available, an assumed layout may be provided to the program.

Visual Inspection of Bridge Deck Surface Using High-Resolution Image

High-resolution bridge deck images are primarily used for visual inspections and permanent documenting of signs of deterioration, previous repairs, and surface wear. Two identical digital cameras mounted on the Robotics Assisted Bridge Inspection Tool (La et al. 2013; Gucunski et al. 2015a, c) are used to take images of the deck surface. As the robot moves along the bridge deck, both cameras continuously take photos in a fully automated manner. All the collected images are stitched into a single or multiple high-resolution image of the bridge deck, depending on the size of the deck. The stitched image can be reviewed at various zoom levels or can be further processed for automatic crack mapping of the bridge deck surface (Lim et al. 2014; Prasanna et al. 2014).

The stitched image displaying a 6×3 m section of the bridge deck (58–64 m and 2–5 m in the longitudinal and transverse directions, respectively) and a closer view of 1.2×1.2 m sections of the bridge deck identifying previous repair and surface cracks are shown in Fig. 10. The resolution of the stitched surface image is approximately 40 pixels per cm (ppcm), which makes the 6×3 m^2 section image of the deck surface a 330-megapixel image.

Integration and Visualization of Multiple NDE Data in a 3D Space

The *NDEFuse* program was developed as a result of collaborative work with the Industrial Motion Art, Vienna, Austria. The program was written in C++ for a Microsoft Windows operating system. The program imports (1) a text-based header file containing general information of a bridge deck, such as deck configuration, thickness, skew, and rebar spacing, among others; (2) text files or Microsoft *Excel* files of numerical matrix of three types of NDE data, IE,

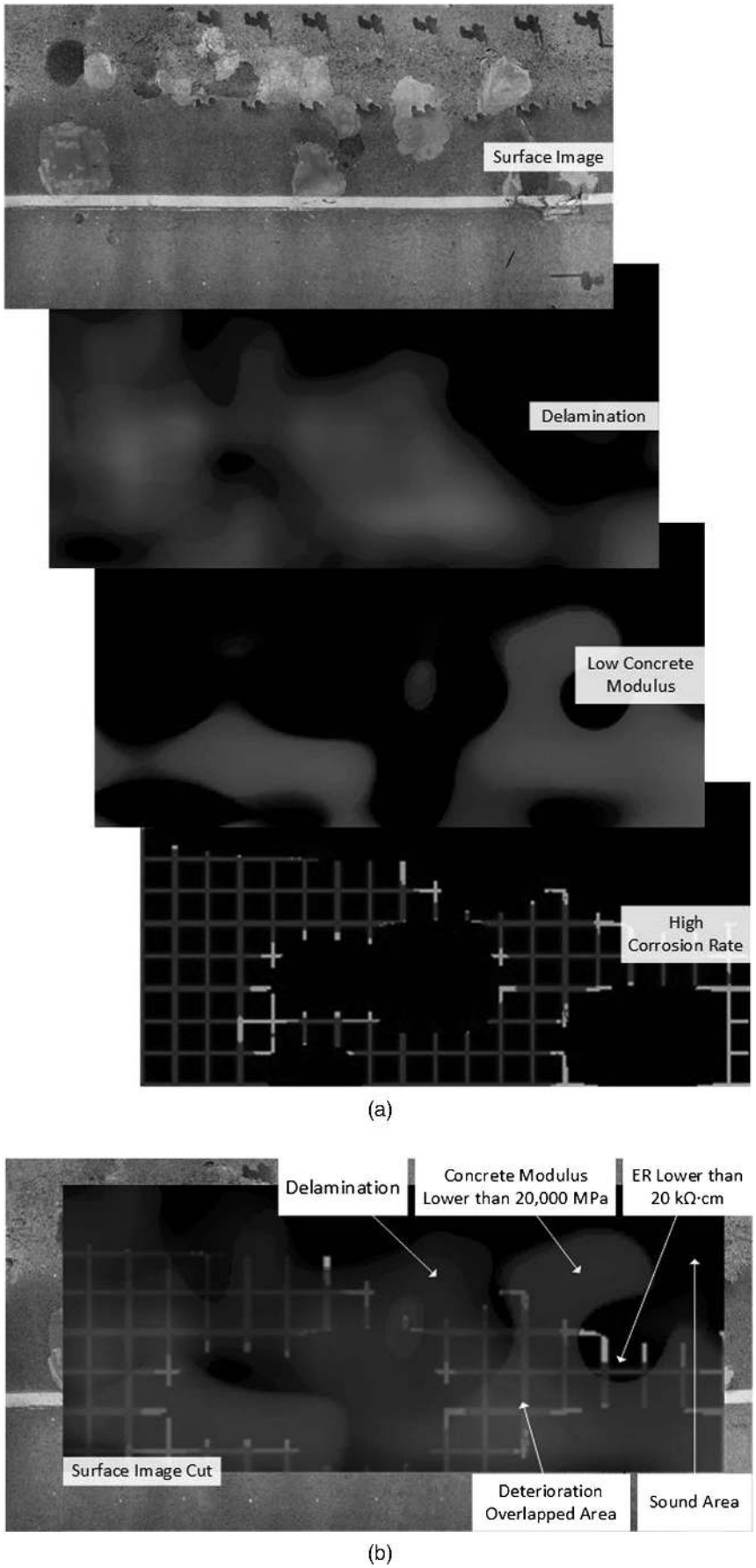

Fig. 11. Integration and visualization of four NDE technologies: (a) visualization of individual NDE survey results; (b) visualization of all NDE survey results

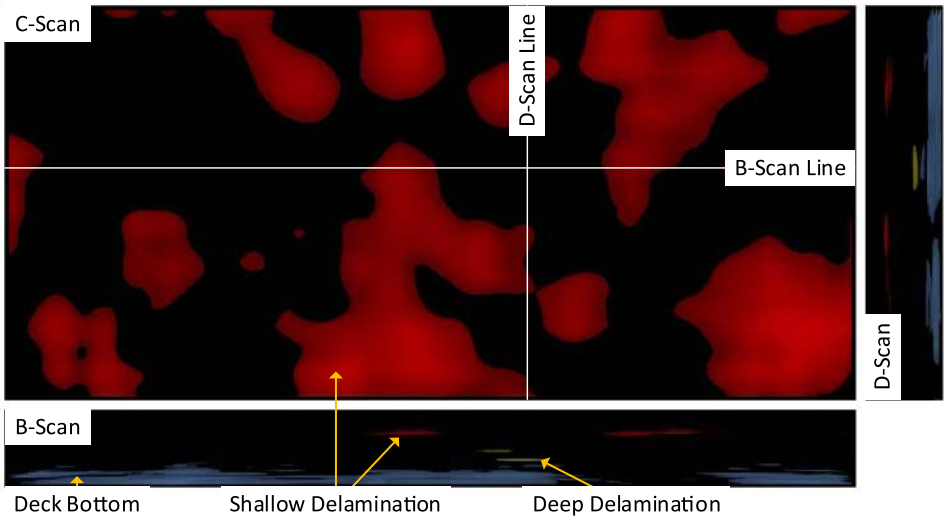

Fig. 12. B-scan, C-scan, and D-scan images of the impact echo survey results

USW, and ER; and (3) an image file of a bridge deck surface. Initially, the program builds boundaries with frames in a 3D space based on the information in the imported header file. The input data for IE, USW, and ER are then processed by the methods described in the preceding section onto the finely discrete 3D grid of voxels, and rendered as a series of texture-mapped planes utilizing *OpenGL*. The stack of closely divided 2D textures forms a hexahedron. The imported surface image is used as an additional planar texture on top (0 in the z-axis) of the volume constructed from the data, and integrated together into a 3D space. Thereby, the *NDEFuse* program integrates the four types of NDE data, IE, USW, ER, and high-resolution image of a bridge deck surface.

In addition to the fundamental role of the conventional 2D condition maps (identifying the location, size, type, and degree of deterioration), the program brings synergistic effects between the individual NDE results. The program also provides visualization of the essential bridge deck information: deck configuration, thickness, skew, concrete cover depth, rebar spacing, and diameter of rebar combined with the NDE results.

Visualization of individual NDE survey results using the *NDEFuse* program for a small section of the bridge deck is shown in Fig. 11(a). The program was set to display only the regions with defects and deterioration, whereas the areas not exhibiting signs of deterioration were set to be completely transparent. This reduced the oversaturation of the image when all the NDE data are presented together. Delamination is presented as gray surfaces, areas with low concrete elastic modulus (less than 20 GPa) are shown as gray clouds, and the top rebar layer is shaded dark gray in the zones with high corrosion rates (ER lower than 20 $k\Omega \cdot cm$). The threshold levels of deterioration and shading settings for each type of the NDE data can be fully customized, which helps users to find the most effective presentation of the results for each NDE technology individually and combined. The combined view of all NDE survey results is shown in Fig. 11(b). The NDE data and the surface image are integrated in the 3D space, where internal defects and deterioration identified by IE, USW, and ER are exposed through the cutting of the surface image. Areas with no considerable deterioration detected from the either of the NDE technologies are presented in black. More importantly, the areas where all NDE technologies detected deterioration have overlapped shades. It can also be observed that the delamination and areas with high corrosion rates are mostly overlapping, indicating that delamination in this region is likely induced by corrosion.

In addition, the program is equipped with a number of interactive and user-friendly functions to enhance visualization of the complex relationship of multiple NDE results in a 3D interface. These include controlling the zoom level and viewing angle to review a region of interest, slicing the 3D space into 2D images displaying the B-scan, C-scan, and D-scan views, and cutting openings in the surface image to expose internal defects and to establish correlations between internal and external (visual) defects and deterioration. The B-scan and D-scan image the results in the vertical planes parallel and perpendicular to the scanning direction, respectively, showing the depth information. The C-scan images the results in the horizontal plane at a selected depth. An example of B-scan, C-scan, and D-scan images of the IE survey results of a small section of the bridge deck is shown in Fig. 12. A shallow delamination, deep delamination, and the bottom of the deck are visualized. The C-scan image is obtained by slicing the 3D volume horizontally at a shallow delamination level in the z-axis, whereas the B-scan and D-scan were sliced vertically along the lines depicted in the figure. The depth in the B-scan and D-scan views has been exaggerated to enable more effective visualization of both delamination and the deck bottom.

A location where a good correlation between internal and external defects can be established is shown in Figs. 13(a and b). Delamination and an area with very high corrosion rate are overlapping below the area where vertical cracks are observed in the surface image. This observation would be a good example of the corrosion-induced delamination. The damaged deck surface might have introduced a pathway to moisture and aggressive agents, such as chloride ions, which caused a reduction in ER, and eventually caused delamination. This hypothesis is also supported by the findings that the depth of delamination in this region (approximately 6–10 cm from the top surface of the deck) matches the top rebar level identified from the bridge deck section drawing. Under the previous surface repair shown in Figs. 13(c and d), delamination was observed, but not accompanied by high corrosion rate. Instead, a low corrosion rate (very high ER of nearly 100 $k\Omega \cdot cm$) is detected. This is most probably because the repair was applied after the delamination has been formed under the surface defect, or the repair material debonded. The high ER observed in this area is expected to be due to the fact that the properties of a new concrete patch are acting as an insulator of the electrical current flow. Therefore, rebar corrosion might have already progressed and delamination has formed underneath the surface repair.

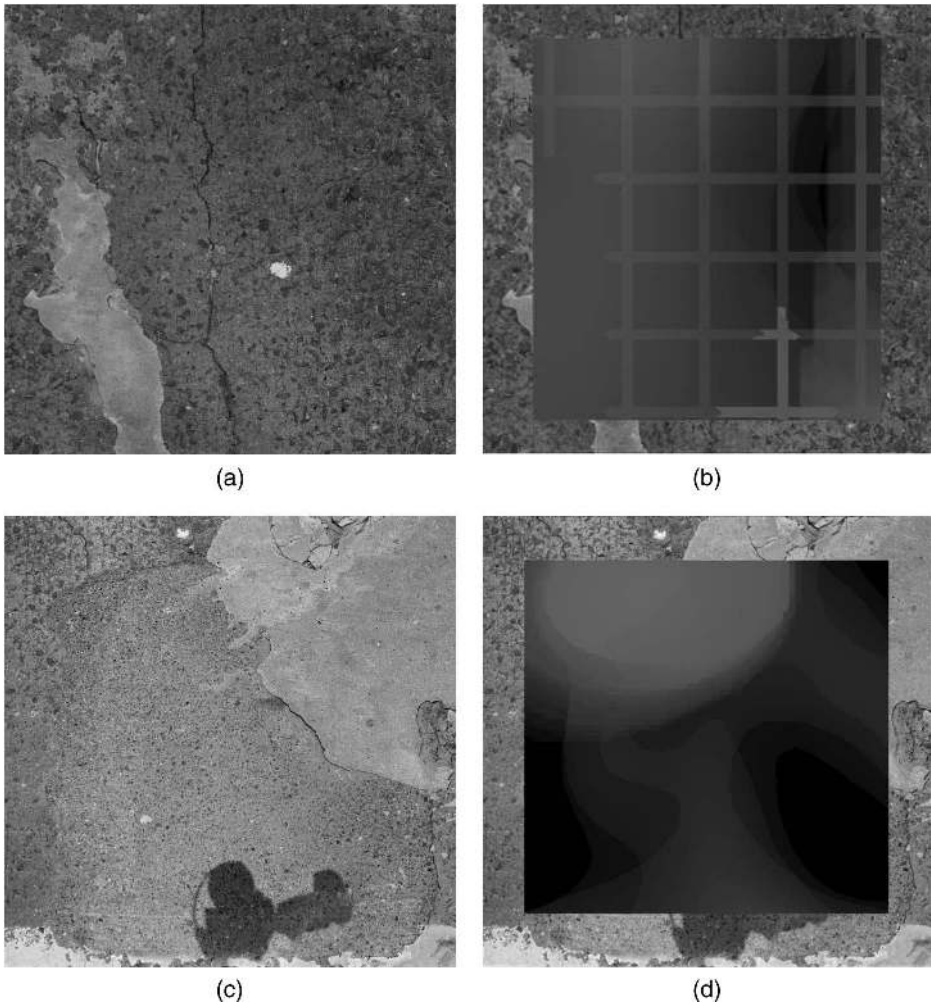

Fig. 13. Effect of surface defects (concrete spalling and previous repair) on the internal condition of the bridge deck: (a) cracked deck surface and (b) exposed internal condition, where delamination and area with very high corrosion rate are overlapped; (c) previous repair and (d) exposed internal condition, where delamination is detected, but with very low corrosion rate

Conclusions

An interactive 3D visualization platform for presentation of multiple NDE data, *NDEFuse*, from concrete bridge deck surveys was developed. The platform enables more effective deck condition presentation and facilitates establishment of correlation between the results from different NDE technologies. The program integrates and visualizes four types of NDE data: delamination data from impact echo; concrete quality evaluation data from USW; corrosion rate estimates from electrical resistivity; and high-resolution imaging of the bridge deck surface for documenting signs of deterioration, previous repairs, and surface wear. Compared with the conventional 2D contour maps, the developed program provides integrated and intuitive visualization of NDE data. Merging and visualizing of multiple NDE data facilitates understanding of the complex relationships between deterioration and defects within the bridge deck, as well as between the internal and visible surface damage. The developed 3D visualization platform can be also used in planning of bridge deck repairs or rehabilitation.

Acknowledgments

The authors sincerely acknowledge the support provided by the Federal Highway Administration through the Long-Term Bridge Performance (LTBP) Program. The authors are also grateful to Mr. Reinhold Fragner of Industrial Motion Art, Vienna, Austria, for the collaboration in the *NDEFuse* program development.

References

ASCE. (2013). "2013 report card for America's infrastructure." Reston, VA.

DHS (Department of Homeland Security). (2010). "Aging infrastructure: Issues, research, and technology." *Buildings and infrastructure protection series*, Washington, DC.

Dyer, T. (2014). *Concrete durability*, CRC Press, Boca Raton, FL.

Gibson, A., and Popovics, J. S. (2005). "Lamb wave basis for impact-echo method analysis." *J. Eng. Mech.*, 10.1061/(ASCE)0733-9399(2005)131:4(438), 438–443.

Gowers, K. R., and Millard, S. G. (1999). "Measurement of concrete resistivity for assessment of corrosion severity of steel using Wenner technique." *ACI Mater. J.*, 96(5), 536–541.

Gucunski, N., et al. (2013). *Nondestructive testing to identify concrete bridge deck deterioration*, Transportation Research Board, Washington, DC.

Gucunski, N., et al. (2015a). "Concrete bridge deck early problem detection and mitigation using robotics." *Proc., Structural Health Monitoring and Inspection of Advanced Materials, Aerospace, and Civil Infrastructure*, San Diego.

Gucunski, N., Kee, S.-H., La, H. M., Basily, B. B., and Maher, A. (2015b). "Delamination and concrete quality assessment of concrete bridge decks using a fully autonomous RABIT platform." *Struct. Monit. Maintenance*, 2(1), 19–34.

Gucunski, N., Kee, S.-H., La, H. M., Basily, B. B., Maher, A., and Ghasemi, H. (2015c). "Implementation of a fully autonomous platform for assessment of concrete bridge decks RABIT." *Proc., Structures Congress 2015*, ASCE, Reston, VA, 367–378.

Gucunski, N., Romero, F., Kruschwitz, S., Feldmann, R., and Parvardeh, H. (2011). "Comprehensive bridge deck deterioration mapping of nine bridges by nondestructive evaluation technologies." Iowa Dept. of Transportation, Ames, IA.

Gucunski, N., Slabaugh, G., Wang, Z., Fang, T., and Maher, A. (2008). "Impact echo data from bridge deck testing: Visualization and interpretation." *Transp. Res. Rec.*, 2050, 111–121.

Gucunski, N., Yan, M., Wang, Z., Fang, T., and Maher, A. (2012). "Rapid bridge deck condition assessment using three-dimensional visualization of impact echo data." *J. Infrastruct. Syst.*, 10.1061/(ASCE)IS .1943-555X.0000060, 12–24.

Kim, J. (2013). "Structural and material health monitoring of cementitious materials using passive wireless conductivity sensors." Ph.D. dissertation, Univ. of Texas, Austin, TX.

Kohl, C., Krause, M., Maierhofer, C., and Wöstmann, J. (2005). "2D- and 3D-visualisation of NDT-data using data fusion technique." *Mater. Struct.*, 38(9), 817–826.

La, H. M., et al. (2013). "Autonomous robotic system for high-efficiency non-destructive bridge deck inspection and evaluation." *Proc., IEEE Int. Conf. on Automation Science and Engineering*, IEEE, New York, 1053–1058.

Langford, P., and Broomfield, J. P. (1987). "Monitoring the corrosion of reinforcing steel." *Constr. Repair*, 1(2), 32–36.

Lim, R. S., La, H. M., and Sheng, W. (2014). "A robotic crack inspection and mapping system for bridge deck maintenance." *IEEE Trans. Autom. Sci. Eng.*, 11(2), 367–378.

Lu, X. (1997). "Application of the Nernst-Einstein equation to concrete." *Cem. Concr. Res.*, 27(2), 293–302.

OpenGL [Computer software]. Khronos Group, Beaverton, OR.

Prasanna, P., et al. (2014). "Automated crack detection on concrete bridges." *IEEE Trans. Autom. Sci. Eng.*, 13(2), 591–599.

Russell, H. G., et al. (2004). "Concrete bridge deck performance." *NCHRP Synthesis 333*, Transportation Research Board, Washington, DC.

Sansalone, M., and Carino, N. J. (1986). "Impact-echo: A method for flaw detection in concrete using transient stress waves." National Bureau of Standards, Washington, DC.

Schickert, M., and Tümmler, U. (2009). "Initial measurement results of an automated ultrasonic scanning and imaging system." *Proc., Non-Destructive Testing in Civil Engineering*, Bauhaus Univ. Weimar, Weimar, Germany.

Surfer 10 [Computer software]. Golden Software, Golden, CO

USDOT (U.S. Department of Transportation). (2014). "2013 status of the nation's highways, bridges, and transit: Conditions & performance." Washington, DC.

Wenner, F., Weibel, E., and Silsbee, F. B. (1915). *Methods of measuring the inductances of low-resistance standards*, U.S. Government Printing Office, Washington, DC.

Whiting, D. A., and Nagi, M. A. (2003). "Electrical resistivity of concrete—A literature review." Portland Cement Association, Skokie, IL.

Wiggenhauser, H. (2009). "Advanced NDT methods for quality assurance of concrete." *Proc., Non-Destructive Testing in Civil Engineering*, BAM Federal Institute for Materials Research and Testing, Berlin.